Computational Methods for Fluid Dynamics Simulations

Alexander Aghili*

July 1, 2026

Abstract

The Navier–Stokes equations express the local conservation of mass, momentum, and energy in a fluid continuum and form the basis of computational fluid dynamics. Their numerical solution requires a choice of spatial discretization and time integrator suited to the flow regime. This article reviews the two principal families of spatial discretization, finite difference methods on structured grids and finite volume methods on arbitrary control volumes, and the explicit Runge–Kutta time integrators that complete the method-of-lines paradigm. Attention is given to the conservation form of the governing equations, to the Riemann-solver-based fluxes that make finite volume methods robust to discontinuities, and to the strong stability preserving Runge–Kutta schemes that retain nonlinear stability bounds in the presence of flux limiting. The trade-offs between the two spatial families, and between classical RK4 and SSP-RK3 in the time domain, are summarized, together with the implicit–explicit splittings used at high Reynolds number on fine grids.

1 Motivation and the Continuum Setting

1.1 Motivation

Fluids appear throughout natural and engineered systems. The atmosphere, the oceans, blood in living organisms, the gases in stellar interiors, and the working fluids in pumps, turbines, and combustion chambers are governed by the same continuum dynamics [2, 6]. Predictive simulation of these flows is a standard application of applied mathematics in engineering and the physical sciences [6, 1]. Applications include the design of wings and rocket nozzles, drag reduction for vehicles and ships, projection of atmospheric and oceanic states, and the design of reactors and separators [1]. In many of these settings, experimental campaigns are impractical or prohibitively expensive, and simulation provides access to the relevant regime.

The mathematical object underlying these applications is the system of Navier-Stokes equations, a set of nonlinear partial differential equations expressing the local conservation of mass, momentum, and energy in a fluid continuum [2, 6]. These equations admit a range of behaviors including laminar flow, shock waves, boundary layers of vanishing thickness, and turbulence with energy distributed across many decades of scale [18]. No general closed-form solution is known, and the question of whether smooth three-dimensional solutions persist for all time is one of the seven Clay Millennium Prize problems. Except in a small set of idealized geometries, the equations must be solved numerically [6].

A standard distinction separates compressible flows, in which density varies with pressure and the energy equation couples to mass and momentum through an equation of state, from incompressible flows, in which $\nabla \cdot \mathbf{u} = 0$ replaces the continuity equation and pressure acts as a Lagrange multiplier enforcing this constraint [3]. The spatial discretizations developed below apply to both, though we focus on the compressible setting where shock capturing motivates the finite volume methods.

*Department of Mathematics, University of California Santa Cruz

A fluid is a continuum that deforms continuously under shear stress [2]. Two complementary descriptions are standard: the Lagrangian view tracks individual fluid parcels along the flow map $\mathbf{X} \mapsto \boldsymbol{\chi}(\mathbf{X}, t)$, while the Eulerian view, which we adopt throughout, fixes a spatial point $\mathbf{x}$ and treats the density ρ, velocity $\mathbf{u}$, and specific total energy E as fields on a domain $\Omega \subset \mathbb{R}^3$. The rate of change of any Eulerian field f following the local flow is given by the material derivative

$$\frac{Df}{Dt} = \frac{\partial f}{\partial t} + (\mathbf{u} \cdot \nabla) f,$$

which separates local temporal variation from advection through a spatially varying field. The two descriptions are linked by the Reynolds transport theorem, which converts material-frame integrals into the fixed-frame conservation laws [2, 6].

1.2 Conserved Variables

The state of a compressible Newtonian fluid is described by five scalar fields [6], collected in the conserved-variable vector

$$\mathbf{Q} = \begin{pmatrix} \rho \\ \rho\mathbf{u} \\ \rho E \end{pmatrix}, \qquad \begin{cases} \rho(\mathbf{x}, t) & \text{mass density} \\ \mathbf{u}(\mathbf{x}, t) = (u, v, w)^T & \text{velocity} \\ E = e + \frac{1}{2}|\mathbf{u}|^2 & \text{specific total energy} \end{cases}$$

where e is the specific internal energy and $\frac{1}{2}|\mathbf{u}|^2$ is the specific kinetic energy [1]. The specific total enthalpy $H = E + p/\rho$ appears in the energy flux, since the work done by pressure on a fluid element moving with velocity $\mathbf{u}$ contributes a flux of $p\mathbf{u}$ to the energy equation, which combines with the internal energy flux $\rho e\mathbf{u}$ to give $\rho H\mathbf{u}$ [1].

Evolving the conserved quantities $(\rho, \rho\mathbf{u}, \rho E)$ rather than the primitive variables $(\rho, \mathbf{u}, p)$ places the governing equations in conservation (divergence) form, which is required for correct shock-capturing and for discrete schemes that respect global balances [16, 17]. The thermodynamic state is closed by an equation of state. For a perfect gas, $p = (\gamma - 1)\rho e$ with $\gamma = c_p/c_v$, so that the pressure and temperature are recovered algebraically from the conserved variables at each time step without solving an additional PDE [1].

2 The Navier-Stokes Equations

2.1 Constitutive Relations

Before writing the conservation laws, we specify how stress and heat flux depend on the state variables [2, 6]. A Newtonian fluid is one in which the viscous stress tensor is a linear, isotropic function of the rate-of-strain tensor $\mathbf{D}$ [2]. Combining isotropy, frame-indifference, and Stokes' hypothesis (vanishing bulk viscosity) gives

$$\boldsymbol{\tau} = \mu\big(\nabla\mathbf{u} + (\nabla\mathbf{u})^T - \tfrac{2}{3}(\nabla \cdot \mathbf{u})\,\mathbf{I}\big)\,,$$

where $\mu > 0$ is the dynamic viscosity and $\mathbf{I}$ is the identity tensor [2]. The trace-free combination on the right ensures that $\boldsymbol{\tau}$ contributes no isotropic pressure, so that all isotropic stress is carried by p.

Heat conduction in a fluid at rest is governed by Fourier's law,

$$\mathbf{q} = -\kappa\,\nabla T,$$

with thermal conductivity $\kappa > 0$ [2]. The two transport coefficients μ and κ are linked by the dimensionless Prandtl number $\mathrm{Pr} = \mu c_p/\kappa$, which is close to 0.72 for air over a wide temperature

range. For an ideal gas the pressure obeys

$$p = (\gamma - 1)\rho e, \qquad T = \frac{p}{\rho R},$$

where R is the specific gas constant and $\gamma = c_p/c_v$ the ratio of specific heats ($\gamma \approx 1.4$ for diatomic gases such as air at moderate temperatures) [1]. These algebraic closures eliminate p, T as independent unknowns: given $\mathbf{Q} = (\rho, \rho\mathbf{u}, \rho E)^T$, every other thermodynamic quantity is recovered without a further PDE.

2.2 Conservation Form

The Navier-Stokes equations express the local balance of mass, momentum, and energy in conservation (divergence) form [2, 6]. On a domain $\Omega \subset \mathbb{R}^3$, they read

$$\begin{aligned}
\frac{\partial \rho}{\partial t} + \nabla \cdot (\rho \mathbf{u}) &= 0, \\
\frac{\partial (\rho \mathbf{u})}{\partial t} + \nabla \cdot (\rho \mathbf{u} \otimes \mathbf{u} + p\,\mathbf{I} - \boldsymbol{\tau}) &= \rho \mathbf{g}, \\
\frac{\partial (\rho E)}{\partial t} + \nabla \cdot [(\rho E + p)\mathbf{u} - \boldsymbol{\tau}\mathbf{u} + \mathbf{q}] &= \rho \mathbf{g} \cdot \mathbf{u},
\end{aligned}$$

where $\mathbf{g}$ is an external body force (typically gravity) and $\otimes$ denotes the outer (tensor) product, so that $(\rho\mathbf{u} \otimes \mathbf{u})_{ij} = \rho u_i u_j$ [6]. Each line states that the time rate of change of a conserved quantity inside a control volume equals the net flux through its boundary plus any volumetric source. Integrating the continuity equation over a fixed volume $V \subset \Omega$ and applying the divergence theorem yields

$$\frac{d}{dt} \int_V \rho \, dV = - \oint_{\partial V} \rho \mathbf{u} \cdot \mathbf{n} \, dS,$$

the integral statement that mass is neither created nor destroyed inside V, only transported across ∂V [17].

Each flux in the momentum and energy equations decomposes into an inviscid part and a viscous part [1]. The inviscid parts $\rho\mathbf{u} \otimes \mathbf{u} + p\mathbf{I}$ and $(\rho E + p)\mathbf{u}$ produce the compressible Euler equations when $\mu = \kappa = 0$. The Euler system is hyperbolic and admits shocks and contact discontinuities [16, 22], the viscous additions $-\boldsymbol{\tau}$ and $-\boldsymbol{\tau}\mathbf{u} + \mathbf{q}$ are second-order in the velocity and temperature gradients, making the full Navier-Stokes system a mixed hyperbolic–parabolic problem [6]. The relative size of inviscid and viscous fluxes is measured by the Reynolds number

$$\mathrm{Re} = \frac{\rho U L}{\mu},$$

where U and L are characteristic velocity and length scales [2]. High-Re flow is convection-dominated and tends to turbulence [18, 20], low-Re flow is diffusion-dominated and tends to be laminar [2].

For incompressible Navier-Stokes, pressure is determined only up to an additive constant unless a Dirichlet condition on p is supplied somewhere on $\partial\Omega$ or the boundary is fully no-slip [3].

3 Computational Approaches to Solving the Equations

There is no closed-form solution of the Navier-Stokes system for generic geometry and boundary data [6]. Instead one constructs a finite-dimensional approximation. Two families of spatial discretization

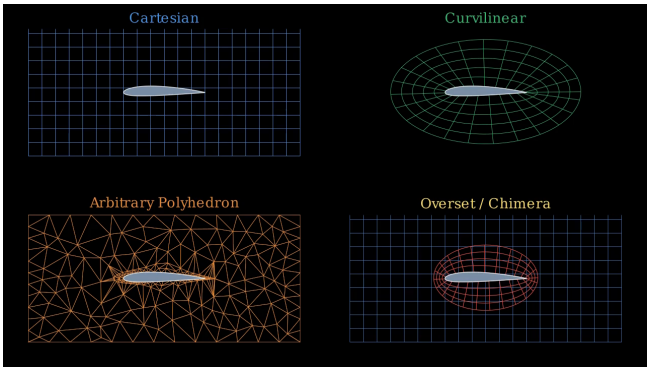

Figure 1: Representative mesh families around an airfoil. A structured Cartesian and body-fitted curvilinear grids that support finite difference stencils, an unstructured polyhedral mesh typical of finite volume schemes, and an overset / chimera arrangement that couples a body-fitted patch with a Cartesian background through interpolation in the overlap region [6].

are standard in practical computational fluid dynamics [6]. Finite difference methods (FDM) approximate derivatives point-wise on structured grids by Taylor expansion. Finite volume methods (FVM) discretize the integral conservation laws on control volumes, with fluxes evaluated at cell faces [17, 22]. After either is applied to the PDE, what remains is a system of ordinary differential equations

$$M\,\dot{\mathbf{U}}(t) = F(\mathbf{U}(t), t)\,,$$

where $\mathbf{U}(t) \in \mathbb{R}^N$ collects the spatial degrees of freedom and M is a mass matrix ($M = I$ for FDM and standard FVM) [10]. This decoupling of space and time is the method of lines, and the ODE above is then advanced by an explicit or implicit time integrator such as a Runge–Kutta or backward differentiation formula [10, 11].

4 Theory of Finite Methods for Spatial Discretization

4.1 The Mesh and the Discrete Problem

Every finite method begins by replacing the continuous domain Ω by a mesh $\mathcal{T}_h$, a finite collection of cells whose union covers Ω [6]. The characteristic cell size is the parameter h, defined either as a uniform grid spacing in the structured case or as $h = \max_{K \in \mathcal{T}_h} \operatorname{diam}(K)$ in the unstructured case. The discretization replaces the infinite-dimensional PDE by a finite-dimensional algebraic problem, and one studies how that approximation behaves as $h \to 0$.

4.2 Consistency, Stability, and the Lax Theorem

Three notions structure the analysis of any spatial discretization.

Definition 4.1 (Consistency)**.** A scheme is consistent of order p if substituting the exact solution into the discrete equations leaves a residual (the truncation error) that is $\mathcal{O}(h^p)$ as $h \to 0$.

Definition 4.2 (Stability)**.** A scheme is stable if the discrete solution operator is uniformly bounded in some appropriate norm, independent of h (and, for time-dependent problems, independent of the time step within a CFL-type restriction).

Theorem 4.3 (Lax equivalence, informal)**.** *For a well-posed linear evolution problem and a consistent finite scheme, stability is necessary and sufficient for convergence.*

In practice, designing a convergent scheme reduces to designing one that is simultaneously consistent and stable. Both criteria are constructive: consistency is established by Taylor expansion of the truncation error, and stability is established by spectral or energy arguments on the discrete operator [10]. The error of a p-th order scheme then decays as $\|u - u_h\| = \mathcal{O}(h^p)$ in the relevant norm.

5 Finite Difference Methods

5.1 Derivation from Taylor Expansion

The finite difference method approximates derivatives by truncating Taylor series [6]. On a uniform one-dimensional grid $x_i = ih$, expanding a smooth function u about x_i gives the two expansions

$$u_{i+1} = u_i + h\,u_i' + \tfrac{h^2}{2}u_i'' + \tfrac{h^3}{6}u_i''' + \tfrac{h^4}{24}u_i^{(4)} + \mathcal{O}(h^5),$$
$$u_{i-1} = u_i - h\,u_i' + \tfrac{h^2}{2}u_i'' - \tfrac{h^3}{6}u_i''' + \tfrac{h^4}{24}u_i^{(4)} + \mathcal{O}(h^5),$$

where primes denote derivatives evaluated at x_i. Subtracting cancels every even-order term,

$$u_{i+1} - u_{i-1} = 2h\,u_i' + \tfrac{h^3}{3}u_i''' + \mathcal{O}(h^5),$$

yielding the second-order central difference for the first derivative,

$$u'(x_i) = \frac{u_{i+1} - u_{i-1}}{2h} - \frac{h^2}{6}u_i''' + \mathcal{O}(h^4) = \frac{u_{i+1} - u_{i-1}}{2h} + \mathcal{O}(h^2)$$

Adding cancels every odd-order term,

$$u_{i+1} + u_{i-1} = 2u_i + h^2 u_i'' + \tfrac{h^4}{12}u_i^{(4)} + \mathcal{O}(h^6),$$

and gives the second-order central difference for the second derivative,

$$u''(x_i) = \frac{u_{i+1} - 2u_i + u_{i-1}}{h^2} - \frac{h^2}{12}u_i^{(4)} + \mathcal{O}(h^4).$$

Higher-order stencils follow from Richardson extrapolation on the same central formula. Letting $D_h u_i = (u_{i+1} - u_{i-1})/(2h)$, the expansion above reads

$$D_h u_i = u_i' + \tfrac{h^2}{6}u_i''' + \tfrac{h^4}{120}u_i^{(5)} + \mathcal{O}(h^6).$$

Replacing h by $2h$ gives an estimate on a wider stencil with a leading error four times as large,

$$D_{2h} u_i = \frac{u_{i+2} - u_{i-2}}{4h} = u_i' + \tfrac{4h^2}{6}u_i''' + \tfrac{16h^4}{120}u_i^{(5)} + \mathcal{O}(h^6),$$

and the combination $\frac{1}{3}(4D_h u_i - D_{2h} u_i)$ cancels the $\mathcal{O}(h^2)$ term to leave the fourth-order central stencil

$$u'(x_i) = \frac{-u_{i+2} + 8u_{i+1} - 8u_{i-1} + u_{i-2}}{12h} + \mathcal{O}(h^4),$$

with leading truncation error $\frac{h^4}{30}u_i^{(5)}$. The same construction extends to arbitrary even order, with the stencil coefficients fixed by matching the Taylor expansion through the desired number of terms [6].

Higher spatial dimensions are handled by tensor products of one-dimensional stencils [6].

5.2 Application to the Navier-Stokes Equations

For the Navier-Stokes system one discretizes the spatial terms in the conservation form component by component [6, 1]. The pressure gradient ∇p, the viscous Laplacian $\nabla \cdot \boldsymbol{\tau}$, and the convective derivative $(\mathbf{u} \cdot \nabla)\mathbf{u}$ each receive their own stencil. The convective term is the difficult one: a central difference is non-dissipative and admits spurious oscillations when the flow develops sharp gradients [6]. Two standard remedies are upwinding, which biases the stencil toward the direction of incoming characteristics [23], and flux limiting, which blends a high-order and a low-order discretization based on a smoothness sensor. Kinetic-energy preserving discretizations [13] provide an alternative route for low-dissipation simulation of compressible turbulence, sidestepping the need for an upwind bias by enforcing discrete energy balances directly.

5.3 The CFL Condition

When the semi-discrete system is advanced by an explicit time step Δt, the scheme is stable only if information cannot propagate further than one cell per step [5]. For a linear advection equation $u_t + a u_x = 0$ this gives the Courant–Friedrichs–Lewy condition

$$\nu := \frac{|a|\,\Delta t}{h} \leq 1.$$

For the compressible Navier-Stokes equations the relevant signal speed is $|\mathbf{u}| + c$ with $c = \sqrt{\gamma p/\rho}$ the speed of sound, and an additional parabolic constraint $\Delta t \leq h^2/(\mu/\rho)$ arises from the viscous terms [6]. The smaller of the two restrictions governs the explicit time step. Implicit schemes remove the CFL restriction at the cost of solving a nonlinear system at every step [11].

6 Finite Volume Methods

6.1 Integral Formulation

The finite volume method [17, 6, 22] takes the conservation form of the equations as its starting point. Partition Ω into a finite set of non-overlapping control volumes $\{K_i\}$ with $\bigcup K_i = \Omega$. Integrating a generic conservation law

$$\frac{\partial \mathbf{q}}{\partial t} + \nabla \cdot \mathbf{F}(\mathbf{q}) = \mathbf{s}(\mathbf{q})$$

over K_i and applying the divergence theorem yields

$$\frac{d}{dt}\int_{K_i} \mathbf{q}\, dV + \oint_{\partial K_i} \mathbf{F}(\mathbf{q}) \cdot \mathbf{n}\, dS = \int_{K_i} \mathbf{s}\, dV.$$

The unknowns are the cell averages

$$\bar{\mathbf{q}}_i(t) = \frac{1}{|K_i|}\int_{K_i} \mathbf{q}(\mathbf{x}, t)\, dV,$$

and the discrete evolution becomes

$$\frac{d\bar{\mathbf{q}}_i}{dt} = -\frac{1}{|K_i|}\sum_{f \in \partial K_i} \hat{\mathbf{F}}_f \cdot \mathbf{n}_f\, |f| + \bar{\mathbf{s}}_i,$$

where $\hat{\mathbf{F}}_f$ is a numerical approximation of the physical flux on face f, $\mathbf{n}_f$ is the outward unit normal, and $|f|$ is the area of the face [17, 22]. This equation is the canonical finite volume semi-discretization and fits the method-of-lines template with M the diagonal matrix of cell volumes.

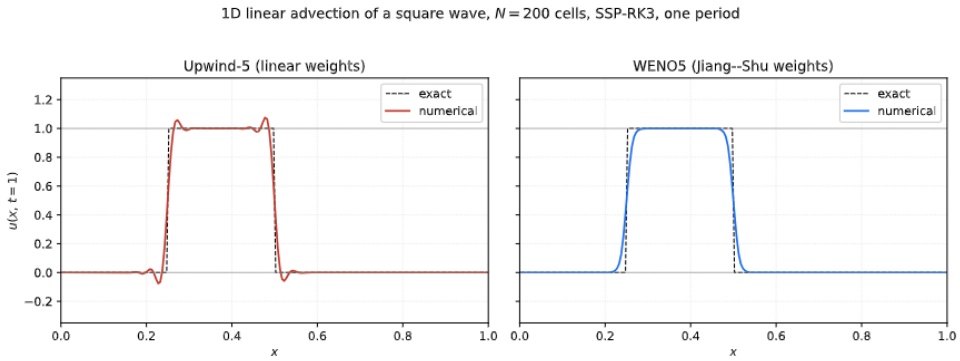

Figure 2: Linear advection of a square wave over one period, $N = 200$ cells, SSP-RK3 in time. The two runs share the same 5th-order upwind stencil, only the weight calculation differs. The linear weights overshoot at each discontinuity, while the Jiang–Shu nonlinear weights detect the jumps through the smoothness indicators and stay monotone, at the cost of a few cells of smearing.

6.2 Local and Global Conservation

Because the face flux $\hat{\mathbf{F}}_f \cdot \mathbf{n}_f$ is shared by exactly two neighboring cells, with opposite normals, summing this equation over all interior cells produces a telescoping cancellation of interior fluxes [17, 16]. What remains is

$$\frac{d}{dt} \sum_i |K_i| \, \bar{\mathbf{q}}_i = - \sum_{f \subset \partial\Omega} \hat{\mathbf{F}}_f \cdot \mathbf{n}_f \, |f| + \sum_i |K_i| \, \bar{\mathbf{s}}_i,$$

the discrete analogue of global conservation. Local conservation, in turn, follows from the consistency of the face flux: $\hat{\mathbf{F}}_f$ depends only on neighbor states, and is used identically by both adjacent cells. This property is the defining feature of FVM, and is required for capturing shocks and other discontinuous solutions of the Euler and Navier-Stokes equations [16, 17, 22].

6.3 Numerical Fluxes and Riemann Solvers

The crux of any finite volume scheme is the choice of $\hat{\mathbf{F}}_f$ [22]. The simplest option is the centered flux $\frac{1}{2}(\mathbf{F}(\mathbf{q}_L) + \mathbf{F}(\mathbf{q}_R))$, where L, R denote the cell states on either side of the face. This is second-order accurate but non-dissipative and unstable for nonlinear hyperbolic problems [17]. Upwinded fluxes are obtained by solving (exactly or approximately) the one-dimensional Riemann problem at the face [7]. Standard choices include the Roe flux [19], the HLL flux [12], and the Godunov flux [7, 22], each trading accuracy against cost and robustness. Higher-order spatial accuracy is achieved by reconstructing $\mathbf{q}_L, \mathbf{q}_R$ from neighboring cell averages by polynomial interpolation, with limiters such as MUSCL [23] or WENO [14] suppressing oscillations near discontinuities.

6.4 Trade-offs Between the Two Methods

The two families differ in how they accommodate complex geometry, in whether they enforce conservation exactly, and in the cost of obtaining high-order accuracy [6]. The following table summarizes the trade-offs that motivate the choice of one family over another in practice:

	FDM	FVM
Geometry flexibility	low	high
Local conservation	indirect	exact
High-order extension	easy on Cartesian grids	hard
Implementation complexity	low	medium

FDM requires a structured grid, either Cartesian or smoothly curvilinear, while FVM permits arbitrary cell shape and thus handles unstructured meshes around complex configurations directly [6]. Additionally, FVM enforces mass, momentum, and energy balance by construction through shared face fluxes that telescope across the mesh [16, 17], whereas FDM recovers these balances only as the truncation error vanishes [17]. Finally, additional nodes in the Taylor expansion raise the order of an FDM stencil at minimal cost on a Cartesian grid [6], while high-order FVM on unstructured meshes requires stencils reaching across multiple cell layers and careful boundary treatment. The asymmetry is why high-order FDM still dominates direct numerical simulation of turbulence in canonical domains [18], while engineering practice for compressible flow on complex geometry has migrated to FVM [6]. Modern discontinuous Galerkin methods [4] retain the Riemann-solver-based interface treatment of FVM while carrying polynomial degrees of freedom inside each cell.

7 Time Discretization

7.1 The Method-of-Lines Framework

The spatial discretizations reduce the Navier-Stokes equations to an autonomous system of ordinary differential equations

$$\dot{\mathbf{U}}(t) = L(\mathbf{U}(t)), \qquad \mathbf{U}(0) = \mathbf{U}_0,$$

where $\mathbf{U}(t) \in \mathbb{R}^N$ collects the spatial degrees of freedom and $L : \mathbb{R}^N \to \mathbb{R}^N$ encodes the discrete divergence of the inviscid and viscous fluxes together with any source terms [10, 6]. A time integrator advances $\mathbf{U}^n \approx \mathbf{U}(t_n)$ to $\mathbf{U}^{n+1} \approx \mathbf{U}(t_n + \Delta t)$ by a fixed pattern of stage-evaluations of L [10].

The choice between explicit and implicit integrators is dictated by stiffness [11]. Convection-dominated regimes place the spectrum of $\partial L/\partial \mathbf{U}$ near the imaginary axis, where explicit Runge–Kutta schemes with bounded stability regions suffice [10]. Viscous and chemically reacting flows introduce strongly negative real eigenvalues that force an explicit step $\Delta t = \mathcal{O}(h^2)$, in such regimes one switches to implicit schemes at the cost of solving a nonlinear system at each step [11, 15]. A classification of stability regions and order conditions is given in Hairer, Nørsett, and Wanner [10] and the companion stiff volume [11].

7.2 Classical Fourth-Order Runge–Kutta

An explicit s-stage Runge–Kutta method computes intermediate slopes $\mathbf{k}_1, \dots, \mathbf{k}_s$ and combines them with weights b_j [10]:

$$\mathbf{k}_j = L\left(\mathbf{U}^n + \Delta t \sum_{l<j} a_{jl}\mathbf{k}_l\right), \qquad \mathbf{U}^{n+1} = \mathbf{U}^n + \Delta t \sum_{j=1}^{s} b_j\, \mathbf{k}_j,$$

the coefficient matrix $A = (a_{jl})$ being strictly lower triangular. The classical four-stage scheme RK4 may be written explicitly as

$$\begin{aligned}
\mathbf{k}_1 &= L(\mathbf{U}^n), \\
\mathbf{k}_2 &= L\big(\mathbf{U}^n + \tfrac{\Delta t}{2}\mathbf{k}_1\big), \\
\mathbf{k}_3 &= L\big(\mathbf{U}^n + \tfrac{\Delta t}{2}\mathbf{k}_2\big), \\
\mathbf{k}_4 &= L(\mathbf{U}^n + \Delta t\, \mathbf{k}_3), \\
\mathbf{U}^{n+1} &= \mathbf{U}^n + \tfrac{\Delta t}{6}(\mathbf{k}_1 + 2\mathbf{k}_2 + 2\mathbf{k}_3 + \mathbf{k}_4).
\end{aligned}$$

The local truncation error is $\mathcal{O}(\Delta t^5)$ per step, yielding fourth-order global accuracy [10]. The linear stability region of RK4 contains a segment of the imaginary axis between $\pm 2\sqrt{2}\,i$, which suits convection-dominated spatial operators whose eigenvalues cluster there [10]. RK4 is a standard explicit integrator for direct numerical simulation of turbulence in smooth domains, where shock-capturing flux limiters are absent and only its linear stability matters [18].

7.3 Strong Stability Preserving Schemes

Classical accuracy criteria are insufficient when the spatial operator includes nonlinear flux limiters or shock-capturing reconstructions, since these are stable only under additional discrete constraints (e.g. a TVD or maximum principle) on the input states. Strong stability preserving (SSP) Runge–Kutta methods [21, 9, 8] guarantee that any such stability property inherited from the forward-Euler step is preserved by the full multi-stage update.

Suppose the forward-Euler step $\mathbf{U}^{n+1} = \mathbf{U}^n + \Delta t\, L(\mathbf{U}^n)$ satisfies $\|\mathbf{U}^{n+1}\| \le \|\mathbf{U}^n\|$ for all $\Delta t \le \Delta t_{\mathrm{FE}}$ in some convex norm, seminorm, or convex functional. A Runge–Kutta scheme is SSP if it can be written as a convex combination of forward-Euler steps [21, 9]:

$$\mathbf{U}^{(j)} = \sum_l \Big(\alpha_{jl}\, \mathbf{U}^{(l)} + \Delta t\, \beta_{jl}\, L(\mathbf{U}^{(l)}) \Big), \qquad \alpha_{jl}, \beta_{jl} \ge 0, \quad \sum_l \alpha_{jl} = 1.$$

The same stability bound then holds under the (generally more restrictive) condition $\Delta t \le c\, \Delta t_{\mathrm{FE}}$, where the SSP coefficient

$$c = \min_{j,l:\, \beta_{jl} > 0} \frac{\alpha_{jl}}{\beta_{jl}}$$

measures the efficiency of the scheme [9, 8].

The three-stage, third-order SSP method of Shu and Osher [21], denoted SSP-RK3, is

$$\begin{aligned} \mathbf{U}^{(1)} &= \mathbf{U}^n + \Delta t\, L(\mathbf{U}^n), \\ \mathbf{U}^{(2)} &= \tfrac{3}{4}\,\mathbf{U}^n + \tfrac{1}{4}\,\mathbf{U}^{(1)} + \tfrac{1}{4}\,\Delta t\, L(\mathbf{U}^{(1)}), \\ \mathbf{U}^{n+1} &= \tfrac{1}{3}\,\mathbf{U}^n + \tfrac{2}{3}\,\mathbf{U}^{(2)} + \tfrac{2}{3}\,\Delta t\, L(\mathbf{U}^{(2)}). \end{aligned}$$

Each stage is a convex combination of forward-Euler updates, so the SSP coefficient is $c = 1$: any monotonicity, TVD, or maximum-principle property of L under forward Euler carries over to SSP-RK3 with no change in the CFL number [9]. This is the property that makes SSP-RK3 the default time integrator in shock-capturing finite volume and discontinuous Galerkin codes [4, 8].

Theorem 7.1 (Optimal-order barrier [9])**.** *There is no four-stage, fourth-order explicit Runge–Kutta method with all $\alpha_{jl}, \beta_{jl} \ge 0$, or equivalently, the SSP coefficient of any fourth-order explicit Runge–Kutta scheme with positive coefficients is zero.*

The barrier explains why no SSP analogue of RK4 exists at the same stage count. Fourth-order accuracy and the positivity of the convex-combination coefficients are incompatible at four stages. Raising the order under the SSP constraint therefore requires an extra stage, and any nominally fourth-order four-stage scheme used with a flux limiter, RK4 included, relies on coefficient cancellations that the SSP analysis cannot accommodate.

7.4 Stability and the Effective CFL

The CFL condition stated previously reflects the linear stability of forward Euler [5]. For an explicit Runge–Kutta scheme with stability region $S \subset \mathbb{C}$, the time-stepped method is stable provided

$$\Delta t\, \sigma(\partial L / \partial \mathbf{U}) \subset S, \tag{1}$$

where $\sigma(\cdot)$ denotes the spectrum [10]. For pure linear advection with second-order central differences the spatial spectrum lies on the imaginary axis, and forward Euler is unconditionally unstable. RK4's imaginary-axis stability $\pm 2\sqrt{2}\,i$ yields the linear CFL bound

$$\nu = \frac{(|\mathbf{u}| + c)\,\Delta t}{h} \leq 2\sqrt{2} \approx 2.83,$$

and SSP-RK3, whose stability region intersects the imaginary axis at $\pm\sqrt{3}\,i$, gives $\nu \leq \sqrt{3}$ [9]. The smaller linear bound of SSP-RK3 is the price paid for nonlinear robustness under flux limiting. Its SSP coefficient $c = 1$ guarantees the same nonlinear stability bound as forward Euler, with no CFL penalty.

The parabolic diffusion constraint $\Delta t \leq h^2\rho/\mu$ remains the binding restriction at high Reynolds number on fine grids, since it is more restrictive than the hyperbolic bound by a factor of $h\,\mathrm{Re}/L$ [6]. This stiffness motivates implicit-explicit splittings [15], in which the diffusive operator is integrated implicitly while the convective operator continues to advance under SSP-RK3 or RK4. The resulting effective time step scales as $\mathcal{O}(h)$ throughout the Reynolds-number range, at the cost of one symmetric positive-definite linear solve per stage.

8 Conclusion

The Navier-Stokes equations express local conservation of mass, momentum, and energy in a Newtonian continuum, and their numerical solution underlies modern computational fluid dynamics [6]. The framework developed here pairs two spatial discretizations, finite difference methods, simple and high-order on structured grids [6], and finite volume methods, conservative by construction and robust to discontinuities through Riemann-solver-based fluxes on arbitrary meshes [17, 22], with two explicit Runge–Kutta integrators: RK4 for smooth, convection-dominated flow on regular grids [10, 18], and SSP-RK3 whenever the spatial operator includes a nonlinear limiter, since it preserves the nonlinear stability bounds of forward Euler at the same CFL number [21, 9]. Contemporary methods such as discontinuous Galerkin [4] build on these foundations, so a working knowledge of the canonical schemes here remains the prerequisite for engaging with the wider literature.

References

[1] John D. Anderson. *Computational Fluid Dynamics: The Basics with Applications*. McGraw-Hill, New York, 1995. 1, 2, 3, 6

[2] George K. Batchelor. *An Introduction to Fluid Dynamics*. Cambridge University Press, Cambridge, 1967. 1, 2, 3

[3] Alexandre J. Chorin. Numerical solution of the Navier–Stokes equations. *Mathematics of Computation*, 22(104):745–762, 1968. 1, 3

[4] Bernardo Cockburn and Chi-Wang Shu. Runge–Kutta discontinuous Galerkin methods for convection-dominated problems. *Journal of Scientific Computing*, 16(3):173–261, 2001. 8, 9, 10

[5] Richard Courant, Kurt Friedrichs, and Hans Lewy. Über die partiellen Differenzengleichungen der mathematischen Physik. *Mathematische Annalen*, 100:32–74, 1928. 6, 9

[6] Joel H. Ferziger and Milovan Perić. *Computational Methods for Fluid Dynamics*. Springer, Berlin, 3rd edition, 2002. 1, 2, 3, 4, 5, 6, 7, 8, 10

[7] Sergei K. Godunov. A difference scheme for numerical computation of discontinuous solutions of equations of fluid dynamics. *Matematicheskii Sbornik*, 47(3):271–306, 1959. 7

[8] Sigal Gottlieb and David I. Ketcheson. *Strong Stability Preserving Runge-Kutta and Multistep Time Discretizations*. World Scientific, Singapore, 2011. 9

[9] Sigal Gottlieb, Chi-Wang Shu, and Eitan Tadmor. Strong stability-preserving high-order time discretization methods. *SIAM Review*, 43(1):89–112, 2001. 9, 10

[10] Ernst Hairer, Syvert P. Nørsett, and Gerhard Wanner. *Solving Ordinary Differential Equations I: Nonstiff Problems*. Springer, Berlin, 2nd edition, 1993. 4, 5, 8, 9, 10

[11] Ernst Hairer and Gerhard Wanner. *Solving Ordinary Differential Equations II: Stiff and Differential-Algebraic Problems*. Springer, Berlin, 2nd edition, 1996. 4, 6, 8

[12] Amiram Harten, Peter D. Lax, and Bram van Leer. On upstream differencing and Godunov-type schemes for hyperbolic conservation laws. *SIAM Review*, 25(1):35–61, 1983. 7

[13] Antony Jameson. Formulation of kinetic energy preserving conservative schemes for gas dynamics and direct numerical simulation of one-dimensional viscous compressible flow in a shock tube using entropy and kinetic energy preserving schemes. *Journal of Scientific Computing*, 34(2):188–208, 2008. 6

[14] Guang-Shan Jiang and Chi-Wang Shu. Efficient implementation of weighted ENO schemes. *Journal of Computational Physics*, 126(1):202–228, 1996. 7

[15] Christopher A. Kennedy and Mark H. Carpenter. Additive Runge–Kutta schemes for convection–diffusion–reaction equations. *Applied Numerical Mathematics*, 44(1–2):139–181, 2003. 8, 10

[16] Peter D. Lax and Burton Wendroff. Systems of conservation laws. *Communications on Pure and Applied Mathematics*, 13(2):217–237, 1960. 2, 3, 7, 8

[17] Randall J. LeVeque. *Numerical Methods for Conservation Laws*. Birkhäuser, Basel, 2nd edition, 1992. 2, 3, 4, 6, 7, 8, 10

[18] Stephen B. Pope. *Turbulent Flows*. Cambridge University Press, Cambridge, 2000. 1, 3, 8, 9, 10

[19] Philip L. Roe. Approximate Riemann solvers, parameter vectors, and difference schemes. *Journal of Computational Physics*, 43(2):357–372, 1981. 7

[20] Pierre Sagaut. *Large Eddy Simulation for Incompressible Flows*. Springer, Berlin, 3rd edition, 2006. 3

[21] Chi-Wang Shu and Stanley Osher. Efficient implementation of essentially non-oscillatory shock-capturing schemes. *Journal of Computational Physics*, 77(2):439–471, 1988. 9, 10

[22] Eleuterio F. Toro. *Riemann Solvers and Numerical Methods for Fluid Dynamics*. Springer, Berlin, 3rd edition, 2009. 3, 4, 6, 7, 10

[23] Bram van Leer. Towards the ultimate conservative difference scheme. V. A second-order sequel to Godunov's method. *Journal of Computational Physics*, 32(1):101–136, 1979. 6, 7